RSC Advances

PAPER

View Article Online
View Journal | View Issue

CrossMark click for updates

Cite this: *RSC Adv.*, 2016, **6**, 96484

# Electro-chemo-mechanical deformation properties of polypyrrole/dodecylbenzenesulfate linear actuators in aqueous and organic electrolyte

A. Kivilo,[a] Z. Zondaka,[a] A. Kesküla,[a] P. Rasti,[b] T. Tamm[a] and R. Kiefer*[ac]

Received 17th August 2016
Accepted 5th October 2016

DOI: 10.1039/c6ra20766a

www.rsc.org/advances

The immobilization of dodecylbenzenesulfonate ($DBS^-$) in polypyrrole (PPy) during electropolymerization is typically expected to lead to cation-driven activity and actuation properties, at least in actuation electrolyte. Here, the complete reversal of the behavior is demonstrated, as the solvent is changed from aqueous to organic while maintaining the same electrolyte – bis(trifluoromethane)sulfonimide lithium salt. Isotonic and isometric electro-chemo-mechanical deformation (ECMD) measurements under cyclic voltammetric and square wave potential measurements yielded strain and stress values in ranges of 9–10% and 0.7–1 MPa, respectively, independent of the solvent. The morphology of PPy/DBS films also changed with the solvent exchange, while elemental analysis confirmed that fluorine atoms from the $TFSI^-$ anions can be found only in the PPy/DBS films operated in organic solvent.

Published on 10 October 2016. Downloaded by Uppsala University on 3/1/2019 8:22:11 AM.

## 1 Introduction

Conducting polymers have been widely studied with several applications in actuators,[1–3] sensors,[4] biomedical devices,[5] and composites,[6] flexible electrode materials,[7] super capacitors,[8] and many more.[9] Applications of conducting polymers in actuators are still not quite on the verge of commercial products, yet. One reason for this relies on the lack of understanding of the factors determining the direction and extent of actuation. In an ideal actuator only a single and well described type of actuation direction (anion or cation-driven) should be established, unfortunately, in most cases mixed ion behaviour has been observed, leading to lack of control and unpredictable changes that take place during redox cycles.[10] Many parameters including polymerization conditions,[11] electrolyte concentration,[12] and solvents[13] influencing the actuation properties have been addressed in the last decades to understand the conducting polymer (CP) actuation mechanism. Several models such as polaron/bipolaron model,[14] model of reversible σ-dimerization[15] and the electrochemically stimulated conformational relaxation (ESCR) model[16] have been introduced in the literature to explain the structural and electronic changes conducting polymers undergo during redox cycles. Linear CP actuators are essentially free standing CP films, shown in the past[17,18] to have up to 30–40% strain and 10 MPa stress, depending on the choice of conducting polymer,[19] influenced by the polymerization conditions[11] and the applied electrolytes.[2] A typical well investigated and known cation-driven actuator is PPy doped with $DBS^-$, where the immobilized anions lead to cation incorporation[2] upon reduction (eqn (1)):

$$\left[(PPy^{n+})(DBS^-)_n\right] + n(Li^+) + m(S) + n(e^-) \underset{ox}{\overset{red}{\rightleftharpoons}} \left[(PPy)^0(DBS^-)_n(Li^+)_n(S)_m\right] \quad (1)$$

Recent work[13] on solvent effects with the $LiClO_4$ electrolyte did reveal that PPy/DBS trilayer bending actuators change their actuation direction to anion-driven when organic solvent was applied. For linear PPy/DBS actuators, it has been shown that the size of anion and cation have an influence on the actuation direction.[2] In this work, we want to characterize the solvent contribution to the behaviour of PPy/DBS linear actuators, focusing on the actuation direction, strain and stress. Consecutive potential cycles, square potential steps at different frequencies will control the oxidation/reduction driven actuation. The results will be discussed and corroborated by scanning electron microscopy (SEM) and energy-dispersive X-ray spectroscopy (EDX) analyses of the films.

## 2 Material and methods

### 2.1 Materials

Sodium dodecylbenzenesulfonate (NaDBS, 99%), ethylene glycol (EG, 99.8%), bis(trifluoromethane)sulfonimide lithium salt (LiTFSI, 99.95%) and propylene carbonate (PC, 99%) were obtained from Sigma-Aldrich and used as supplied. Pyrrole (Py,

[a]*Intelligent Materials and Systems Lab, Institute of Technology, University of Tartu, Nooruse 1, 50411 Tartu, Estonia. E-mail: rudolf.kiefer@ut.ee*

[b]*iCV Research Group, Institute of Technology, University of Tartu, Nooruse 1, 50411 Tartu, Estonia*

[c]*Ton Duc Thang University, Faculty of Applied Sciences, 19 Nguyen Huu Tho, Tan Phong, Ho Chi Minh City, Vietnam*



This journal is © The Royal Society of Chemistry 2016

Published on 10 October 2016. Downloaded by Uppsala University on 3/1/2019 8:22:11 AM.

≥98%) from Sigma-Aldrich was distilled at reduced pressure prior use and stored at low temperature under argon atmosphere. Milli-Q+ water was used for solutions.

### 2.2 Polymerization of PPy/DBS

PPy/DBS was polymerized galvanostatically at 0.1 mA $cm^{-2}$ (40 000 s at −20 °C) in a two-electrode cell with a stainless steel mesh counter electrode and a stainless steel sheet working electrode (18 $cm^2$) in 0.2 M NaDBS, 0.2 M Py in EG : water (1 : 1) mixture. The films were peeled off from the stainless steel sheet after the polymerization, washed with ethanol to remove excess monomers and washed with water to remove excess NaDBS. The films were stored in 0.2 M NaDBS EG : water 1 : 1 solution. The thickness of the PPy/DBS films was measured with a micrometer.

### 2.3 ECMD (isotonic and isometric) measurements

PPy/DBS films were cut in dimensions of 20 mm length and 1 mm width. The films were connected on the force sensor (TRI202PAD, Panlab) with a fixed arm that served as a working electrode in the linear muscle analyzer set up.[20] Platinum sheet was used as the counter electrode and Ag/AgCl (3 M KCl) as the reference electrode in the measurement cell with 0.2 M solutions of LiTFSI in either water or propylene carbonate. The in-house ECMD measurement setup has the advantage of a movable force sensor instead of a steady one, allowing to determine the mass (mg) needed to change the film length per 1 μm (the $k$ factor, mg $\mu m^{-1}$). The in-house control software applies the $k$ factor to calculate the corresponding length changes of the films. For PPy/DBS films in aqueous and PC solutions, the $k$ factor was determined to be 178 mg $\mu m^{-1}$ and 125 mg $\mu m^{-1}$, respectively. The initial length of the films between the clamps was 1 mm. The force (isometric, constant length) and length changes (isotonic, constant force of 4.9 mN) under the applied electrical signal were measured in real time with the in-house software. The strain $\varepsilon$ in % was obtained from the formula $\varepsilon = \Delta L/L \times 100$. The difference of the length change $\Delta L$ = response to $L - L_1$ where $L$ is the original length of the film and $L_1$ the changed length obtained from the isotonic ECMD measurements. Within a voltage range of 0.6 V to −0.8 V, the cyclic voltammetry (scan rate 5 mV $s^{-1}$) and the chronoamperometry at frequencies 0.005 Hz, 0.01 Hz, 0.025 Hz, 0.05 Hz and 0.1 Hz were performed.

### 2.4 Characterization of the films (SEM, EDX)

PPy/DBS films before and after actuations in different solvents but the same electrolyte were analyzed with SEM and EDX (Helios NanoLab 600, FEI). The PPy/DBS films reduced/oxidized (±0.8 V for 5 min) under different solvent conditions were analyzed, to determine the ions present in the cross-section area of the films (broken in liquid nitrogen).

## 3 Results

### 3.1 Cyclovoltammetric ECMD measurements

Fig. 1a and b reveal that PPy/DBS films show purely cation-driven actuation in aqueous solution with strain of 7.7% and

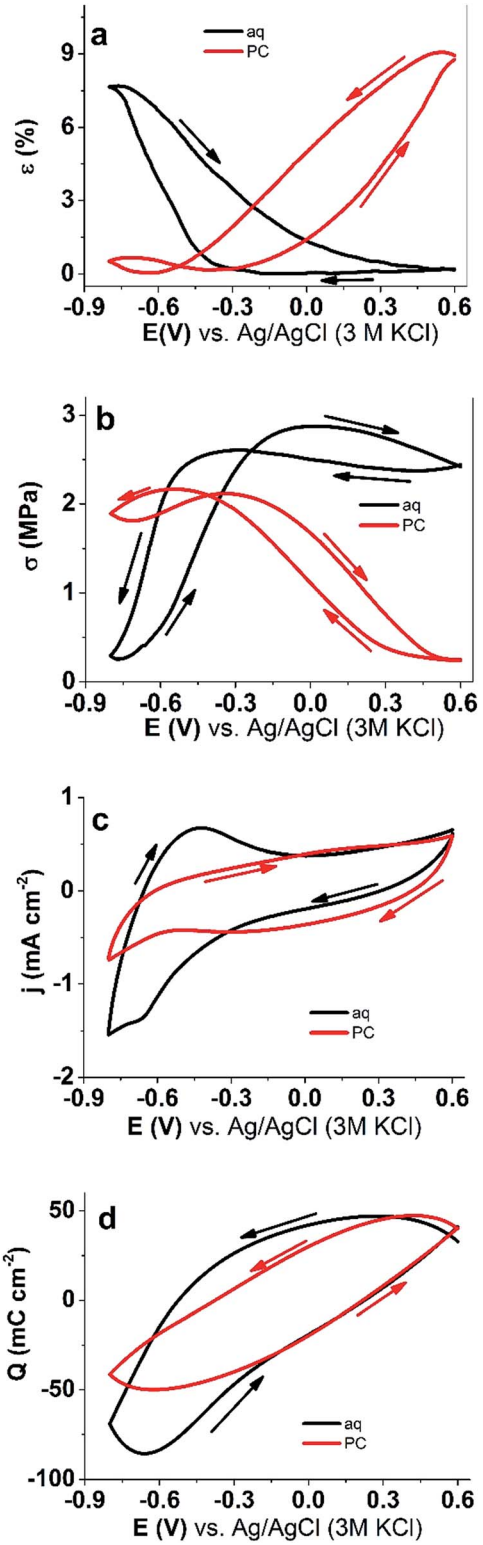


Fig. 1 Cyclic voltammetry (scan rate 5 mV $s^{-1}$, 0.2 M LiTFSI, *vs.* Ag/AgCl (3 M KCl) reference electrode 5th cycle) under steady state condition (charging/discharging in balance) in potential range 0.6 to −0.8 V of PPy/DBS films in different solvents (black: aqueous, aq; red: propylene carbonate, PC). Comparison of strain curves (a) and stress curves (b) against potential; (c) voltammetric responses and (d) coulovoltammetric ($Q/E$) response.

Published on 10 October 2016. Downloaded by Uppsala University on 3/1/2019 8:22:11 AM.

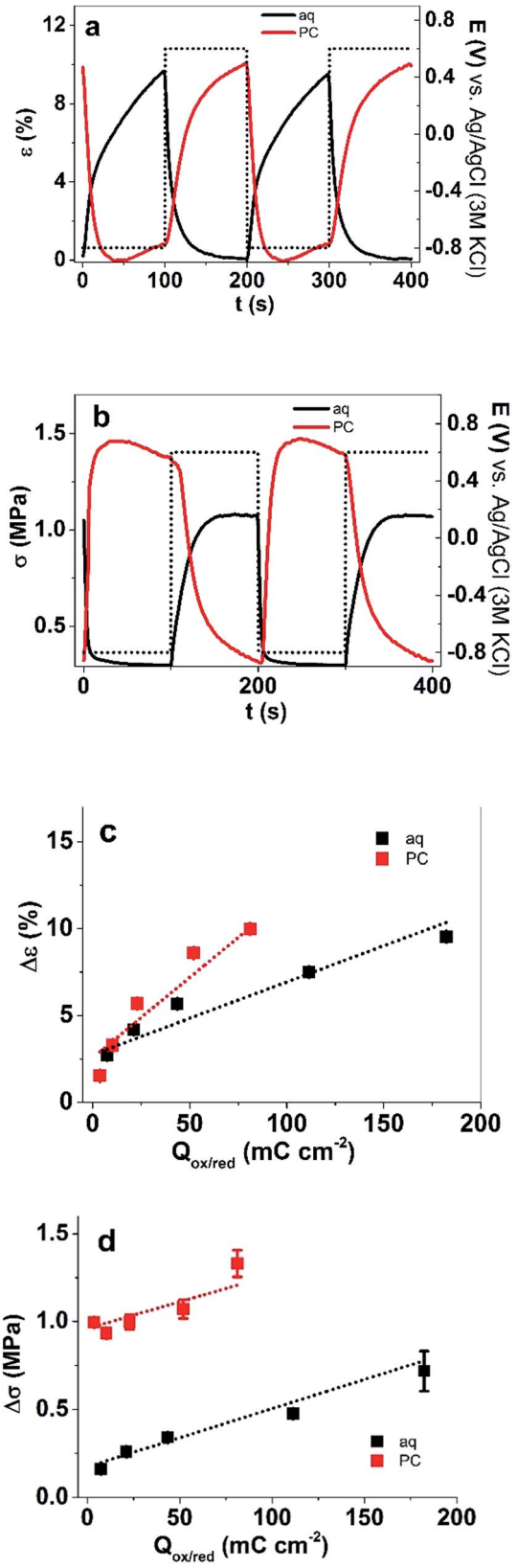


Fig. 2 Chronoamperometric ECMD measurements (square wave potential steps) at frequency 0.005 Hz of PPy/DBS films in same electrolyte but different solvents: water (black) and PC (red); 0.6 to −0.8 V. (a) Strain response (2 cycles, 0.005 Hz) *vs.* time, (b) stress response (2 cycles, 0.005 Hz) *vs.* time. (c) Strain and (d) stress as a function of oxidation/reduction charge at frequency range 0.005–0.1 Hz.

stress of 1.65 MPa. Applying propylene carbonate as the solvent led to the opposite actuation direction (almost completely anion driven, strain at 9%, stress at 2.2 MPa), agreeing with previously observed trend for bending trilayer actuators,[13] explained by $Li^+$–$DBS^-$ couples staying inside PPy network with undissociated character in addition to the larger solvation shell of $Li^+$ in PC as compared to water. Another factor for the change in the mobile ion species relies on the character of the solvent which in case for PC is of higher viscosity, impacting the dynamics considerably.[21] The higher viscosity of the solvent and the hydrophilic/hydrophobic nature of the electrolyte have an impact on cation and anion mobility during the redox cycles in view of polymer–electrolyte and polymer–polymer phase. Therefore, we assume that the anion driven actuation in PC is caused by the combination of two effects: altered mobility of ions (described by solvation number, $o$ and $p$ in eqn (2)), and pair-forming Li–DBS salt. Eqn (1) has, therefore, to be modified for anion exchange effect in PPy/DBS type of actuators (eqn (2)).

$$\left[(\mathrm{PPy})^{n+}(\mathrm{DBS}^-)_m(\mathrm{Li}^+)_m(\mathrm{PC})_{(o+p)}(\mathrm{TFSI}^-)_n\right] + n(\mathrm{e}^-)_{\mathrm{metal}} \underset{\mathrm{ox}}{\overset{\mathrm{red}}{\rightleftharpoons}} \left[(\mathrm{PPy})(\mathrm{DBS}^-)_m(\mathrm{Li}^+)_m(\mathrm{PC})_o\right] + n\mathrm{TFSI}^- + p\mathrm{PC} \quad (2)$$

Nevertheless, a small extent of cation involvement can be observed in Fig. 1a and b; assumed to be accompanied by a small part of $TFSI^-$ anions entrapped inside the PPy network during the redox cycles.

The current density potential curve at Fig. 1c is revealing that much higher current densities are obtained in aqueous solvent with a large oxidation peak at −0.43 V and a small reduction peak at −0.66 V. The current density of PPy/DBS in propylene carbonate is just about half of that in water, with a broad oxidation wave at 0.45 V. The coulovoltammetric charge density potential loops (Fig. 1d) showed that the charging/discharging is in balance[22] for the chosen potential range. The shape of the coulovoltammogram gives also information about structural changes[23] appearing during the reversible redox cycles.

### 3.2 Square wave potential steps ECMD measurements

Conducting polymer actuators follow faradaic processes, where the consumed charge is in relation to the extent of actuation (strain and stress). The ECMD responses of square wave potential steps (0.6 to −0.8 V) of PPy/DBS films in different solvents were investigated at different applied frequencies (0.005–0.1 Hz). The strain and stress curves of two consecutive cycles at frequency 0.005 Hz are presented in Fig. 2a and b. The integration of chronoamperometric *I*–*t* curves gives the strain and stress as a function of the consumed charge for the redox processes, as seen in Fig. 2c and d.

The PPy/DBS actuators show nearly equal strain in PC and aqueous solvent, in range of 9–10%, again with clear cation activity in aqueous solution, and mainly anion activity in PC. The small expansion at reduction for PPy/DBS in propylene carbonate can be observed in Fig. 2a and b. We assume that some $TFSI^-$ anions become immobilized in the PPy network,

 This journal is © The Royal Society of Chemistry 2016

Published on 10 October 2016. Downloaded by Uppsala University on 3/1/2019 8:22:11 AM.

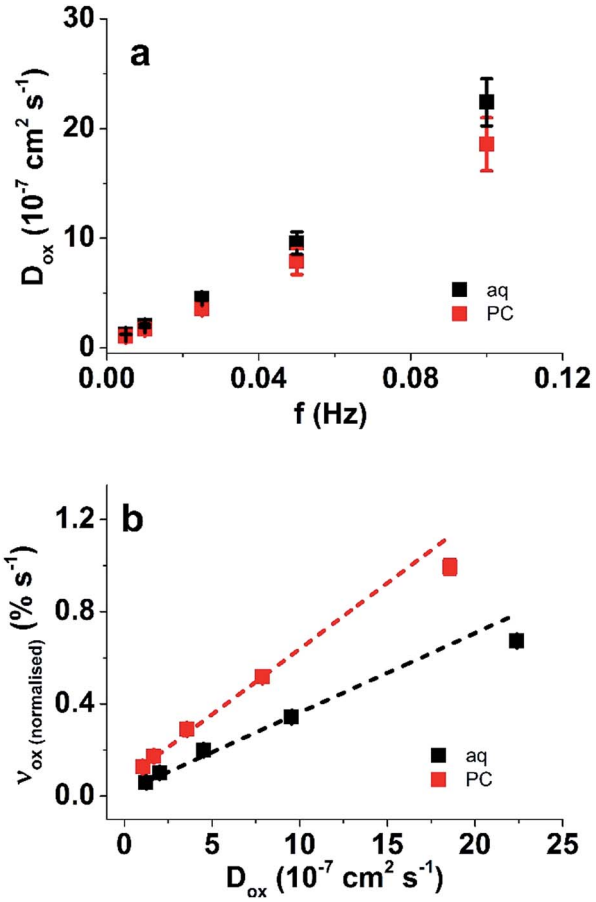


Fig. 3 Diffusion coefficients calculated from eqn (3) and (4), by addressing the chronoamperometric current density time curves of PPy/DBS films in different solvent (same electrolyte LiTFSI): water (black), PC (red) at oxidation. (a) The diffusion coefficient *vs.* applied frequency and (b) the actuation speed $\nu$ (% $s^{-1}$) *vs.* diffusion coefficient *D*. The actuation speed for aqueous electrolyte is normalized (absolute values instead of the originally negative ones, corresponding to the cation expulsion).

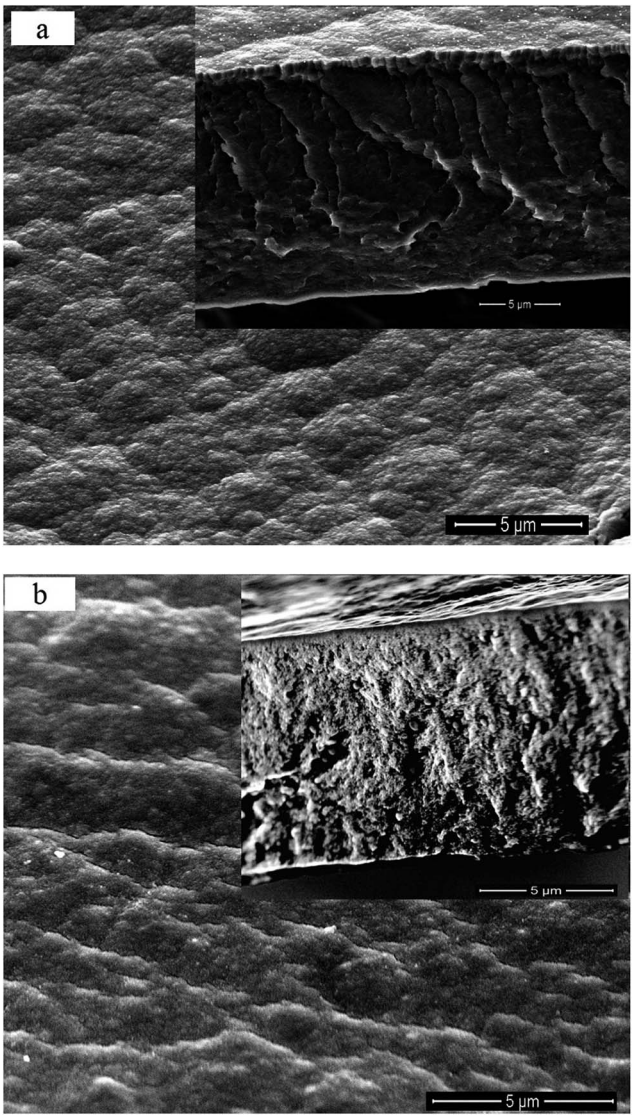


Fig. 4 SEM micrographs (scale bar 5 μm) of PPy/DBS surface (inset – cross section) at oxidized (0.8 V) state in different solvents but same electrolyte (LiTFSI) (a) aqueous solution, (b) PC solution.

forcing a small amount of $Li^+$ cation ingress for compensation at reduction. A similar phenomenon has been observed for $CF_3SO_3^-$ ions in PPy/$CF_3SO_3$ linear actuators, where a more mixed actuation mode was detected.[10] Fig. 2b shows the comparison of the stress of PPy/DBS linear films in different solvents, which is 30% higher (1.08 MPa) in PC solution than in the aqueous solution (0.7 MPa). The coulovoltammetric responses (Fig. 2c and d) describe a faradaic actuator: the strain and stress follow a linear dependency on the consumed charge. The higher stress and strain values of PPy/DBS films in PC solvent are reflecting in Fig. 2c and d, revealing that just about half of charge density of oxidation/reduction is needed for a two-fold increase in strain or stress, in comparison to the aqueous electrolyte.

In earlier studies,[24] different reasons have been proposed why in LiTFSI–PC no cations are exchanged during redox cycles. One possible reason is the solvation number of $Li^+$/PC found in range 4–5.[24] It has been assumed that $Li^+$ ions do not cross the polymer electrolyte interface carrying the full solvent shell with them. Therefore, partially unshelled $Li^+$ ions paired with $DBS^-$ anions in PPy/DBS give rise to the induction of osmotic pressure difference between polymer–electrolyte interfaces, manifested by the huge volume change of PPy/DBS films.[25] Considering that the solvation number of $TFSI^-$ ions in PC solvent is about 2,[26] the much smaller (solvated) $TFSI^-$ anions dragged into the PPy/DBS polymer at oxidation can occupy new locations. The coupling of $Li^+$ and $DBS^-$ ions inside of PPy[27] was assumed to take place in organic solvent such as PC or acetonitrile, as observed in PPy/DBS trilayer bending actuators.[13] The higher viscosity and lower dielectric constant of propylene carbonate is assumed to be responsible for the low dissociation of ions inside PPy films.[28] Changing to aqueous solvent, the solvation number of $Li^+$ ions is found in range of 5–6 (ref. 29) while for $TFSI^-$ ions, due to the delocalized charge and larger size, no solvation number was found.[21] The immobilized $DBS^-$ ions in

Published on 10 October 2016. Downloaded by Uppsala University on 3/1/2019 8:22:11 AM.

PPy lead to $Li^+$ cation incorporation while it is assumed that the $TFSI^-$ anions have no contribution to the reversible volume change.

The rate of ion transport is controlled, through the Faraday's law, by the ion diffusion constant through the PPy network. The ESCR model, including both electrochemical and polymeric structural aspects gives the possibility to get the diffusion coefficient in those swelling/shrinking systems from the chronoamperometric responses:[30]

$$\ln\left[1 - \frac{Q}{Q_t}\right] = -bt \quad (3)$$

where $Q_t$ is the total charge consumed during the time $t$, calculated from the integration of the current–time curve of the chronoamperometric experiment, and $Q$ the charge consumed by each point of time. The diffusion coefficient $D$ is included in $b$ ($h$ is the thickness of the polymer film):

$$D = \frac{bh^2}{2} \quad (4)$$

Plotting $\ln\left[1 - \frac{Q}{Q_t}\right]$ *versus* $t$ provides the $b$[30] as the slope, and together with the film thickness, it gives (eqn (4)) the diffusion coefficient. Fig. 3a presents the evolution of the diffusion coefficients of the anion (PC, TFSI) or cation ($H_2O$, Li) in the PPy–DBS swelling/shrinking films at different frequencies. Fig. 3b shows the strain rate (% $s^{-1}$) at oxidation (normalized for aqueous solvent) against the diffusion coefficient.

Higher frequencies bring along higher diffusion coefficients (Fig. 3a): lower frequencies consume higher redox charges (longer oxidation and reduction times) originating in deeper shrinking/compaction/relaxation/swelling states, while high frequencies only allow soft shrinking/swelling processes.

At lower frequency (0.1 Hz), the highest $D$ ($22.4 \times 10^{-7}$ $cm^2$ $s^{-1}$) corresponds to $Li^+$ diffusion through the dense aqueous PPy/DBS. The $TFSI^-$ diffusion coefficient is always a little bit lower through PC, reaching $18 \times 10^{-7}$ $cm^2$ $s^{-1}$ (0.1 Hz), which can be attributed to either the higher viscosity of PC (2.53 mPa s for PC *vs.* 0.89 mPa s for water), but also to the different interaction type: $Li^+$ cations pair with immobilized anions while $TFSI^-$ anions neutralized the charge of $PPy^{n+}$ in the oxidized state.

The strain rate ($v$) of the linear movement at lower frequencies is nearly under linear control of the frequency dependent average diffusion coefficient ($D$) of the exchanged counter-ions (Fig. 3b) across the swelling/shrinking conducting polymer. In PC, the PPy/DBS film is more swollen; therefore the $TFSI^-$ ions can enter and travel faster in the PPy/DBS network, which is reflected by the higher strain rate, as seen in Fig. 3b. The slope value of the linear fit for the PPy/DBS actuation rate (Fig. 3b) is showing 60% higher value (0.057% $cm^{-2}$) in PC, compared to the 0.034% $cm^{-2}$ in aqueous solution. It may be concluded that although the diffusion coefficient of $TFSI^-$ ions in PC is lower than that of $Li^+$ in water, the effect of swelling rate (expansion) of PPy/DBS in PC solvent is higher. Therefore, ion diffusion coefficients are not the only parameter controlling the strain rates, both the diffusion coefficients and the host matrix properties (both partly dependent on the solvent properties) need to be considered as well as the characteristics of the mobile species themselves.

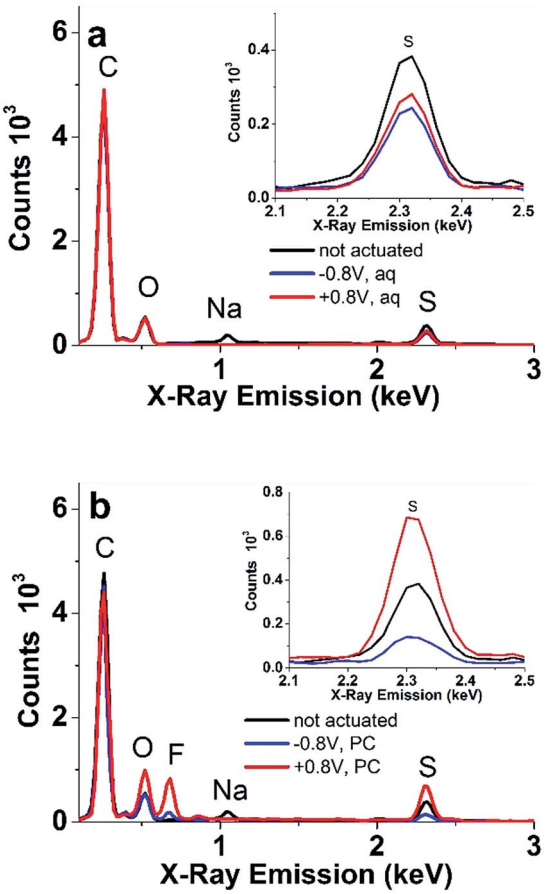


Fig. 5 EDX spectra (inset sulphur peak) of cross sections PPy/DBS films (not actuated, right after polymerization, black), after actuation, reduced (−0.8 V, 5 min, blue), and oxidized at (0.8 V, 5 min, red) in different solvents (same electrolyte LiTFSI) of (a) aqueous and (b) propylene carbonate solutions. $Li^+$ ions were not detectable under EDX.

### 3.3 SEM and EDX analysis

In the previous sections it was shown that the actuation direction of PPy/DBS films depends on the solvent (cation or anion driven). SEM was used to investigate the effect of the different solvents (same electrolyte) to the morphology; the micrographs are presented in Fig. 4.

The typical surface morphology (inset shows dense compaction) of PPy/DBS after actuation in aqueous electrolyte can be observed in Fig. 4a. For PPy/DBS films after actuation in PC electrolyte, the surface morphology has changed to a more swollen state (Fig. 4b), with cross-section (inset) having less dense appearance.

To analyze the ion content of PPy/DBS films before and after actuation in different solvents, EDX measurements from the cross section of the films were made, and presented in Fig. 5.

 This journal is © The Royal Society of Chemistry 2016

Published on 10 October 2016. Downloaded by Uppsala University on 3/1/2019 8:22:11 AM.

The small Na peak at 1.04 keV appearing in Fig. 5a and b of fresh films is a residue of the PPy/DBS deposition. The sulphur peak at 2.315 keV in Fig. 5a (inset) identifies that $DBS^-$ anions are present in the PPy network independent of the solvent applied. PPy/DBS films actuated in PC electrolyte (Fig. 5b) showed a fluoride peak at 0.68 keV, the much larger intensity at oxidation than reduction referring to $TFSI^-$ mobility. The increase of the sulphur and the oxygen peaks at 0.52 keV for oxidized PPy/DBS films actuated in PC are also due to the $TFSI^-$ incorporation. A low-intensity fluoride peak in Fig. 5b testifies that some part of the $TFSI^-$ anions become entrapped during redox cycling. The complete lack of fluoride, together with virtually constant sulphur and oxygen intensities for the aqueous electrolyte films confirm the purely cation-active nature of the films.

# 4 Conclusions

The behavior of PPy/DBS films in solutions of the same electrolyte (LiTFSI) but different solvents: water and propylene carbonate was the subject of this study. ECMD studies revealed that in aqueous solvent, cation-driven actuation (9% strain, 0.7 MPa) took place due to solvated $Li^+$ ion incorporation during reduction (eqn (1)). On the contrary, in propylene carbonate, largely anion-dominated activity was observed (9.8% strain, 1.08 MPa). EDX and SEM results confirmed that in PC solvent $TFSI^-$ ions were the exchanged species. Therefore, ionic species of the electrolyte alone do not determine the actuation direction, rather the nature of the solvent influences electrolyte–polymer interactions. In PC solution, the diffusion coefficient of the active species was found to be lower in comparison to aqueous solution; while contrastingly, the actuation rate in PC was faster than in aqueous solution, meaning that diffusion coefficients (alone) do not determine actuation speed – conducting polymers are faradaic actuators, where the extent in strain and stress are in relation to the charge densities which are independent of the actuation direction but in dependence from the applied solvent.

# Acknowledgements

The work was supported by Estonian Research Council Grant IUT20-24 and PUT638.

# References

1 R. Kiefer, R. Temmer, T. Tamm, J. Travas-Sejdic, P. A. Kilmartin and A. Aabloo, *Synth. Met.*, 2013, **171**, 69–75.
2 N. Aydemir, P. A. Kilmartin, J. Travas-Sejdic, A. Kesküla, A.-L. Peikolainen, J. Parcell, M. Harjo, A. Aabloo and R. Kiefer, *Sens. Actuators, B*, 2015, **216**, 24–32.
3 E. W. H. Jager, E. Smela, O. Ingana and O. Inganäs, *Science*, 2000, **290**, 111–114.
4 Y. A. Ismail, J. G. Martínez, A. S. Al Harrasi, S. J. Kim and T. F. Otero, *Sens. Actuators, B*, 2011, **160**, 1180–1190.
5 A. Gelmi, A. Cieslar-Pobuda, E. de Muinck, M. Los, M. Rafat and E. W. H. Jager, *Adv. Healthcare Mater.*, 2016, 1–10.
6 R. J. Lee, R. Temmer, T. Tamm, A. Aabloo and R. Kiefer, *React. Funct. Polym.*, 2013, **73**, 1072–1077.
7 U. Vanamo and J. Bobacka, *Electrochim. Acta*, 2014, **122**, 316–321.
8 A. Izadi-Najafabadi, D. T. H. Tan and J. D. Madden, *Synth. Met.*, 2005, **152**, 129–132.
9 E. Smela, *Adv. Mater.*, 2003, **15**, 481–494.
10 R. Kiefer, S. Y. Chu, P. A. Kilmartin, G. A. Bowmaker, R. P. Cooney and J. Travas-Sejdic, *Electrochim. Acta*, 2007, **52**, 2386–2391.
11 R. Kiefer, G. A. Bowmaker, P. A. Kilmartin and J. Travas-Sejdic, *Electrochim. Acta*, 2010, **55**, 681–688.
12 L. Valero, T. F. Otero and J. G. Martínez, *ChemPhysChem*, 2014, **15**, 293–301.
13 R. Kiefer, J. G. Martinez, A. Kesküla, G. Anbarjafari, A. Aabloo and T. F. Otero, *Sens. Actuators, B*, 2016, **233**, 328–336.
14 X. Chen and O. Inganäs, *J. Phys. Chem.*, 1996, **100**, 15202–15206.
15 R. Kiefer, D. G. Weis, A. Aabloo, G. Urban and J. Heinze, *Synth. Met.*, 2013, **172**, 37–43.
16 T. F. Otero, H. Grande and J. Rodriguez, *J. Phys. Chem. B*, 1997, **101**, 8525–8533.
17 S. Hara, T. Zama, S. Sewa, W. Takashima and K. Kaneto, *Chem. Lett.*, 2003, **32**, 576–577.
18 L. Bay, K. West, P. Sommer-Larsen, S. Skaarup and M. Benslimane, *Adv. Mater.*, 2003, **15**, 310–313.
19 S. Hara, T. Zama, W. Takashima and K. Kaneto, *J. Mater. Chem.*, 2004, **14**, 1516.
20 Z. Zondaka, R. Valner, T. Tamm, A. Aabloo and R. Kiefer, *RSC Adv.*, 2016, **6**, 26380–26385.
21 G. Orädd, L. Edman and A. Ferry, *Solid State Ionics*, 2002, **152–153**, 131–136.
22 T. F. Otero, M. Marquez and I. J. Suarez, *J. Phys. Chem. B*, 2004, **108**, 15429–15433.
23 T. F. Otero and J. G. Martinez, *Adv. Funct. Mater.*, 2014, **24**, 1259–1264.
24 P. M. Dziewoński and M. Grzeszczuk, *J. Phys. Chem. B*, 2010, **114**, 7158–7171.
25 X. Wang and E. Smela, *J. Phys. Chem. C*, 2009, **113**, 369–381.
26 R.-S. Kühnel and A. Balducci, *J. Phys. Chem. C*, 2014, **118**, 5742–5748.
27 K. Perera, K. P. Vidanapathirana and M. A. K. L. Dissanayake, *Sri Lankan J. Phys.*, 2007, **8**, 39–45.
28 J. Ko, S. Kim and I. Chung, *Synth. Met.*, 1995, **69**, 139–140.
29 Z. Wang, W. Gao, X. Huang, Y. Mo and L. Chen, *J. Raman Spectrosc.*, 2001, **32**, 900–905.
30 T. F. Otero and J. G. Martinez, *J. Solid State Electrochem.*, 2011, **15**, 1169–1178.